RadioGraphics

Advanced MR Imaging Techniques in the Diagnosis of Intraaxial Brain Tumors in Adults[1]

Riyadh N. Al-Okaili, MD • Jaroslaw Krejza, MD, PhD[2] • Sumei Wang, MD • John H. Woo, MD • Elias R. Melhem, MD, PhD

ONLINE-ONLY CME

See www.rsna.org/education/rg_cme.html.

LEARNING OBJECTIVES

After reading this article and taking the test, the reader will be able to:

- List the most common intraaxial brain tumors in adults.
- Describe the typical advanced MR imaging features of common intraaxial brain tumors in adults.
- Classify common intraaxial tumors in adults by integrating various MR imaging techniques.

TEACHING POINTS

See last page

Intraaxial brain masses are a significant health problem and present several imaging challenges. The role of imaging is no longer limited to merely providing anatomic details. Sophisticated magnetic resonance (MR) imaging techniques allow insight into such processes as the freedom of water molecule movement, the microvascular integrity and hemodynamic characteristics, and the chemical makeup of certain compounds of masses. The role of the most commonly used advanced MR imaging techniques—perfusion imaging, diffusion-weighted imaging, and MR spectroscopy—in the diagnosis and classification of the most common intraaxial brain tumors in adults is explored. These lesions include primary neoplasms (high- and low-grade), secondary (metastatic) neoplasms, lymphoma, tumefactive demyelinating lesions, abscesses, and encephalitis. Application of a diagnostic algorithm that integrates advanced MR imaging features with conventional MR imaging findings may help the practicing radiologist make a more specific diagnosis for an intraaxial tumor.

Abbreviations: ADC = apparent diffusion coefficient, FLAIR = fluid-attenuated inversion-recovery, NAA = N-acetylaspartate, rCBV = relative cerebral blood volume, rTBV = relative tumor blood volume, WHO = World Health Organization

RadioGraphics 2006; 26:S173–S189 • **Published online** 10.1148/rg.26si065513 • **Content Codes:** MR NR OI

[1]From the Department of Radiology, University of Pennsylvania School of Medicine, 3400 Spruce St, Dulles 2, Philadelphia, PA 19104. Received May 17, 2006; revision requested June 14 and received July 10; accepted July 13. All authors have no financial relationships to disclose. **Address correspondence to** E.R.M. (e-mail: *Elias.Melhem@uphs.upenn.edu*).

[2]**Current address:** Department of Radiology, Gdansk Medical University, Gdansk, Poland.

Introduction

Intracranial tumors are a significant health problem. The annual incidence of primary and secondary central nervous system neoplasms ranges from 10 to 17 per 100,000 persons. The American Cancer Society and the Primary Brain Tumors in the United States Statistical Report projected that in 2005 in the United States, an estimated 12,760 deaths from intracranial tumors would occur, and that an estimated 43,800 new cases of primary nonmalignant and malignant central nervous system tumors would be diagnosed, respectively.

Imaging plays an integral role in intracranial tumor management. Magnetic resonance (MR) imaging in particular has emerged as the imaging modality most frequently used to evaluate intracranial tumors, and it continues to have an ever-expanding, multifaceted role. In general, the role of MR imaging in the workup of intraaxial tumors can be broadly divided into tumor diagnosis and classification, treatment planning, and posttreatment surveillance.

In addition to conventional MR imaging techniques, a variety of advanced techniques have found their place in clinical practice or are the subject of intense research. These advanced techniques offer more than the anatomic information provided by the conventional MR imaging sequences. They generate physiologic data and information on chemical composition. The current advanced techniques include perfusion imaging, diffusion-weighted imaging (including diffusion-tensor imaging), MR spectroscopy, blood oxygen level–dependent (BOLD) imaging, and the largely experimental molecular imaging. Currently, the first three techniques are more commonly used.

Discrimination of extraaxial and intraaxial brain tumors is relatively easy with only anatomic imaging; however, the major diagnostic challenge is to reliably, noninvasively, and promptly differentiate intraaxial tumors to avoid biopsy and follow-up imaging studies. Integration of diagnostic information from advanced MR imaging techniques can further improve the classification accuracy of conventional anatomic imaging.

This article focuses on the role of the most commonly used advanced MR imaging techniques—perfusion imaging, diffusion-weighted imaging, and MR spectroscopy—for the diagnosis and classification of the most common intraaxial brain tumors in adults. We conclude by presenting a practical diagnostic algorithm that integrates advanced MR imaging features to help the practicing radiologist make a more specific diagnosis for an intraaxial tumor.

Advanced MR Imaging Features of Common Intraaxial Tumors

In the largest stereotactic brain biopsy series, the most common intraaxial brain masses were high-grade primary neoplasms (36% of cases), low-grade primary neoplasms (33%), metastases (8%), lymphoma (5%), demyelinating and inflammatory conditions (3%), infarcts (2%), and abscesses (1%) (1). In the largest stereotactic brain biopsy series, to our knowledge, of nonenhancing brain lesions, the following pathologic conditions were encountered: gliomas, tumefactive demyelinating lesions, and encephalitis (2). Thus herein, we provide a review of the advanced MR imaging features of the following common intraaxial tumors and tumorlike processes in adults: primary neoplasms (high- and low-grade), secondary (metastatic) neoplasms, lymphoma, tumefactive demyelinating lesions, abscesses, and encephalitis.

The location of advanced imaging interrogation can influence the findings, and, unless otherwise indicated, the imaging features described are from solid portions of the lesions. In addition, as in any imaging study, an understanding of limitations and confounding factors is essential to avoid misinterpretation. The features described in this article do not apply for hemorrhagic lesions.

Primary (Non-lymphomatous) Neoplasms

The most common primary brain neoplasms are of glial origin. Low-grade glial neoplasms occur most often in patients aged 20–40 years, whereas high-grade glial lesions occur in older adults who tend to have shorter survival. Currently, high-grade glial neoplasms are differentiated from low-grade ones by pathologic evidence of increasing cellular atypia, nuclear pleomorphism, neovascular proliferation, and necrosis.

MR Spectroscopy.—The typical proton MR spectroscopic features for primary neoplasms are elevated peaks of lipid, lactate, choline, and myo-inositol and reduced NAA signal, summarized in the Table and illustrated in Figures 1–6.

Typical Advanced MR Imaging Features of Intraaxial Brain Tumors

MR Imaging Feature	Neoplasms			Tumefactive Demyelinating Lesion	Abscess*	Encephalitis
	Primary	Secondary	Lymphoma			
MR spectroscopy						
Lipid signal (ppm)	Elevated at 0.9 and 1.3, especially with high-grade lesion	Elevated at 0.9 and 1.3	Elevated at 0.9 and 1.3	. . .	. . .	. . .
Lactate signal (ppm)	Elevated at 1.33, especially with high-grade lesion	Elevated at 1.33	Elevated at 1.33	. . .	Elevated at 1.33	Elevated at 1.33
NAA signal (ppm)	Reduced at 2.02, more so with high-grade lesion	Reduced or absent at 2.02	Reduced at 2.02	Reduced at 2.02	Absent at 2.02	Reduced at 2.02
Choline signal (ppm)	Elevated at 3.2, more so with high-grade lesion	Elevated at 3.2	Elevated at 3.2	Elevated at 3.2, especially with acute lesions	Absent at 3.2	Elevated at 3.2
Myoinositol signal (ppm)	Elevated at 3.55, more so with gliomatosis and low-grade lesion	. . .	. . .	. . .	. . .	Elevated at 3.55
Diffusion-weighted imaging: ADC value	Variable, 0.82–2.73 × 10^{-3} mm^2/sec	Elevated	Reduced	Reduced (crescent or concentric areas) for acute lesions; elevated for chronic lesions	Markedly reduced	Variable
Perfusion imaging: rTBV value	Tends to increase with tumor grade	Elevated	Low, compared with primary high-grade neoplasms; high, relative to toxoplasmosis	Low	Low	Unknown

*Other typical MR spectroscopic features include elevated signals for amino acid (at 0.9 ppm), alanine (at 1.47 ppm), acetate (at 1.92 ppm), pyruvate (at 2.37 ppm), and succinate (at 2.40 ppm), and absent creatine signal (at 3.0 ppm).

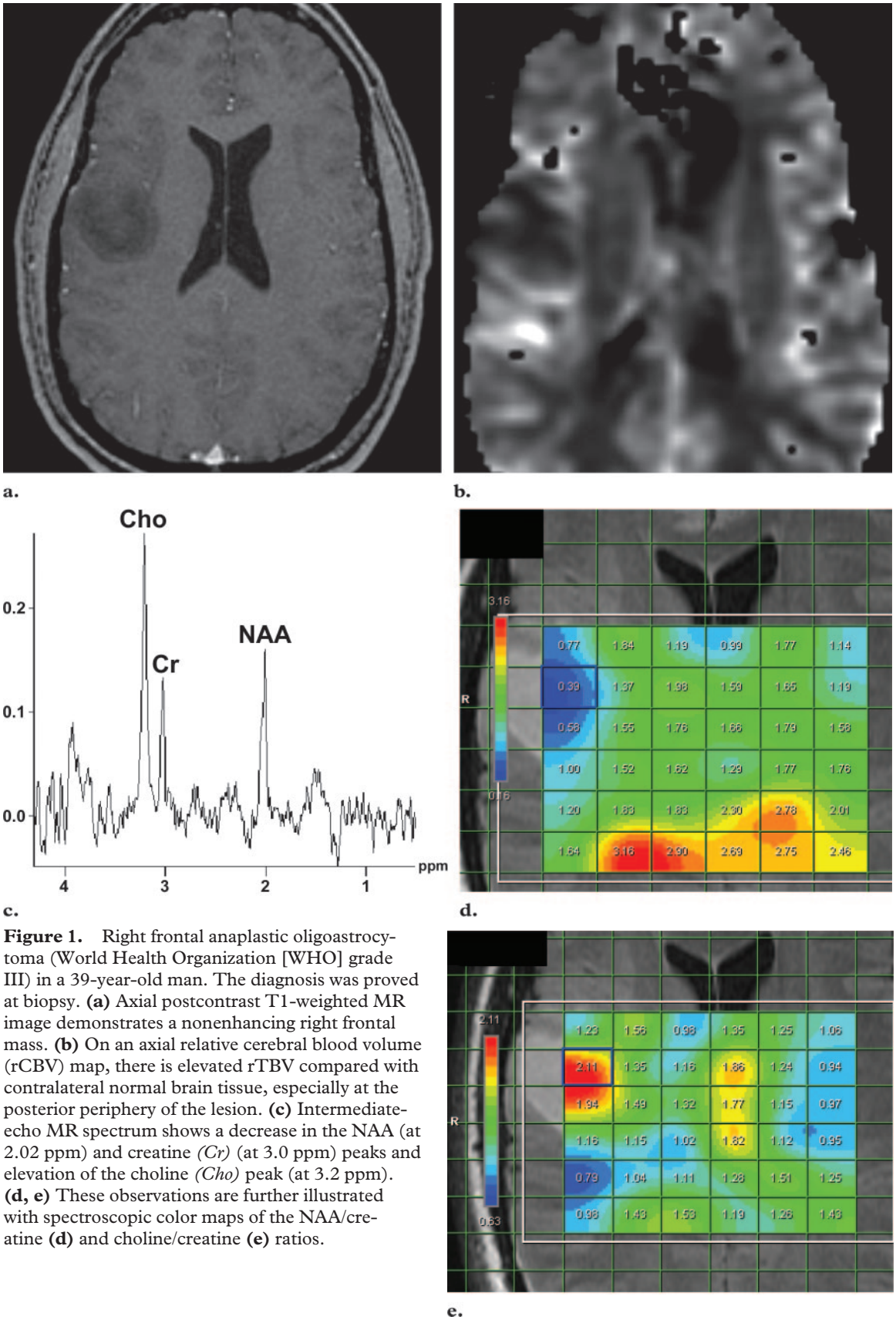

Figure 1. Right frontal anaplastic oligoastrocytoma (World Health Organization [WHO] grade III) in a 39-year-old man. The diagnosis was proved at biopsy. **(a)** Axial postcontrast T1-weighted MR image demonstrates a nonenhancing right frontal mass. **(b)** On an axial relative cerebral blood volume (rCBV) map, there is elevated rTBV compared with contralateral normal brain tissue, especially at the posterior periphery of the lesion. **(c)** Intermediate-echo MR spectrum shows a decrease in the NAA (at 2.02 ppm) and creatine *(Cr)* (at 3.0 ppm) peaks and elevation of the choline *(Cho)* peak (at 3.2 ppm). **(d, e)** These observations are further illustrated with spectroscopic color maps of the NAA/creatine **(d)** and choline/creatine **(e)** ratios.

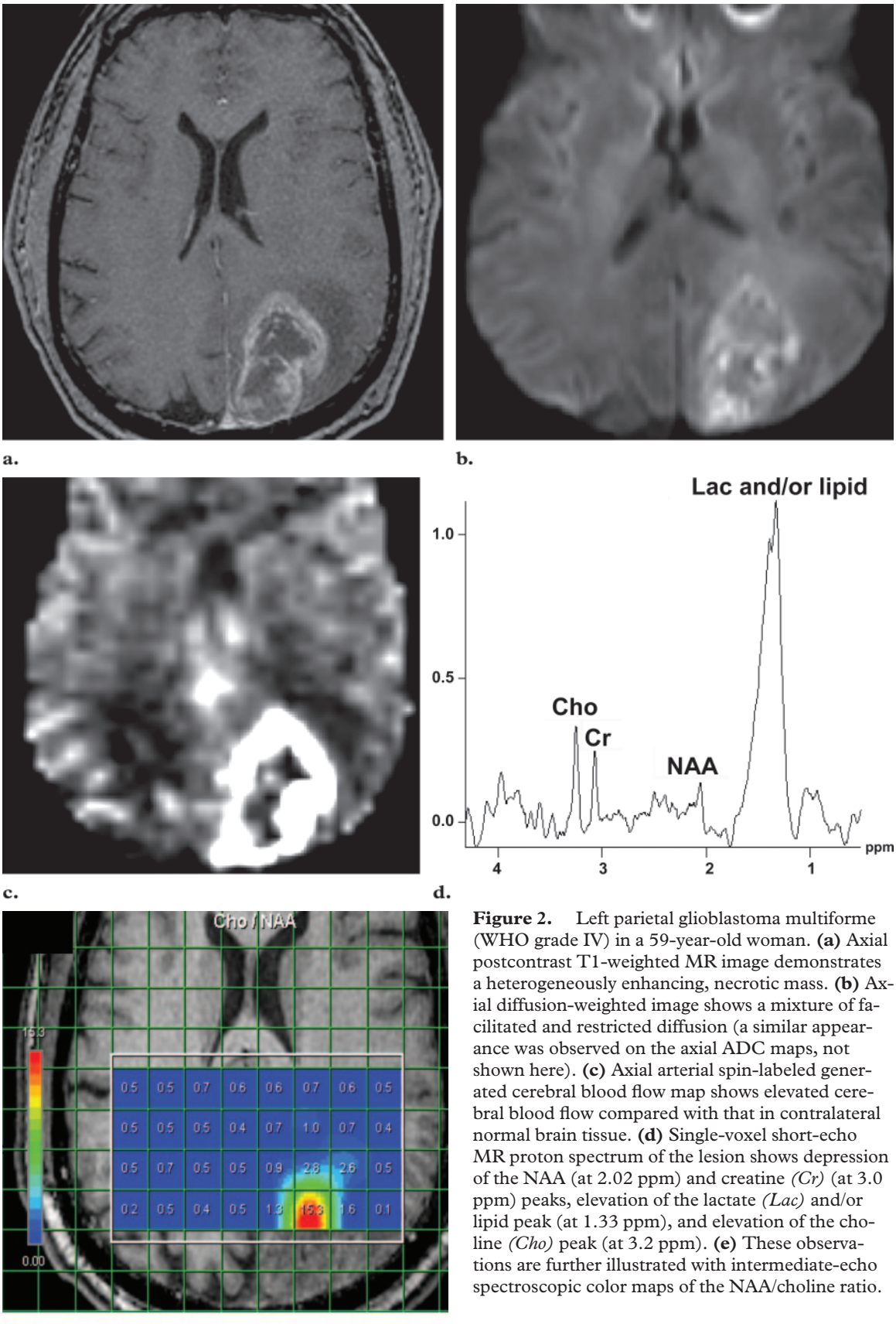

Figure 2. Left parietal glioblastoma multiforme (WHO grade IV) in a 59-year-old woman. **(a)** Axial postcontrast T1-weighted MR image demonstrates a heterogeneously enhancing, necrotic mass. **(b)** Axial diffusion-weighted image shows a mixture of facilitated and restricted diffusion (a similar appearance was observed on the axial ADC maps, not shown here). **(c)** Axial arterial spin-labeled generated cerebral blood flow map shows elevated cerebral blood flow compared with that in contralateral normal brain tissue. **(d)** Single-voxel short-echo MR proton spectrum of the lesion shows depression of the NAA (at 2.02 ppm) and creatine *(Cr)* (at 3.0 ppm) peaks, elevation of the lactate *(Lac)* and/or lipid peak (at 1.33 ppm), and elevation of the choline *(Cho)* peak (at 3.2 ppm). **(e)** These observations are further illustrated with intermediate-echo spectroscopic color maps of the NAA/choline ratio.

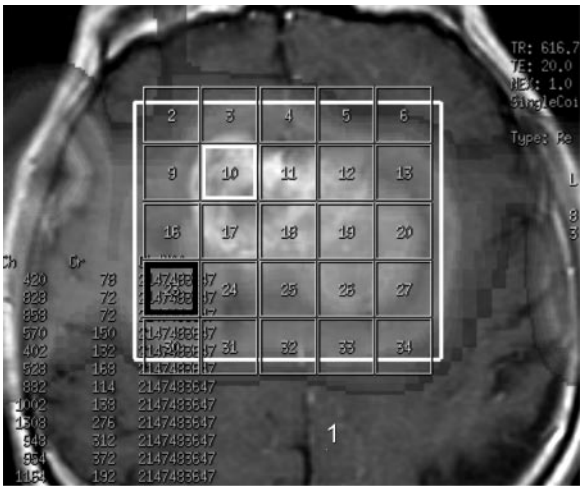

a.

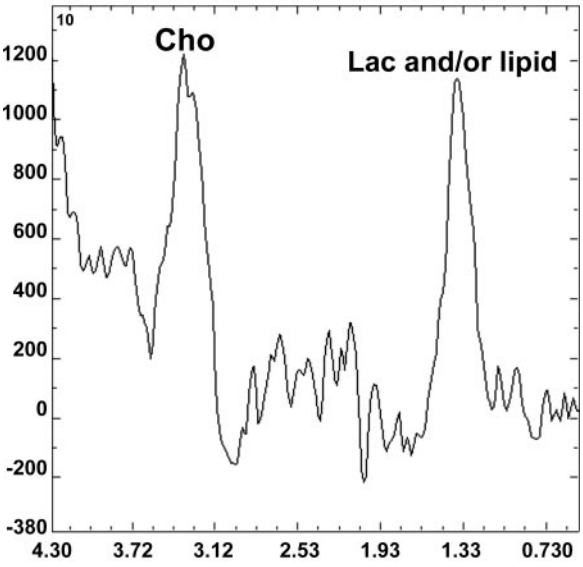

b.

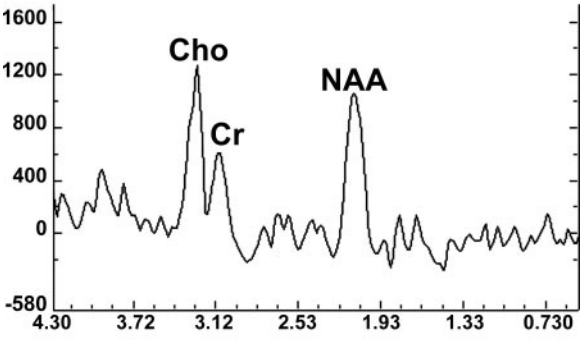

c.

Figure 3. Bifrontal glioblastoma multiforme (WHO grade IV) in a 79-year-old woman. **(a)** Axial postcontrast T1-weighted MR image with overlying spectroscopic grid demonstrates a heterogeneously enhancing, necrotic mass. **(b, c)** Multivoxel short-echo MR proton spectra show depression of the NAA (at 2.02 ppm) and creatine *(Cr)* (at 3.0 ppm) peaks, elevation of the lactate *(Lac)* and/or lipid peak (at 1.33 ppm), and elevation of the choline *(Cho)* peak (at 3.2 ppm) within the enhancing portion of the mass, as seen in voxel 10 (outlined with a white frame in **a**). There is also evidence of peritumoral infiltration, as voxel 23 (outlined with a black frame in **a**)— which is beyond the enhancing portion of the lesion—shows the choline/NAA ratio >1.

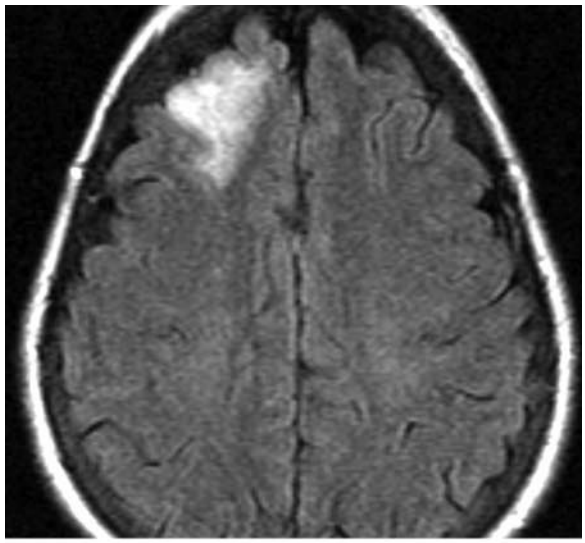

a.

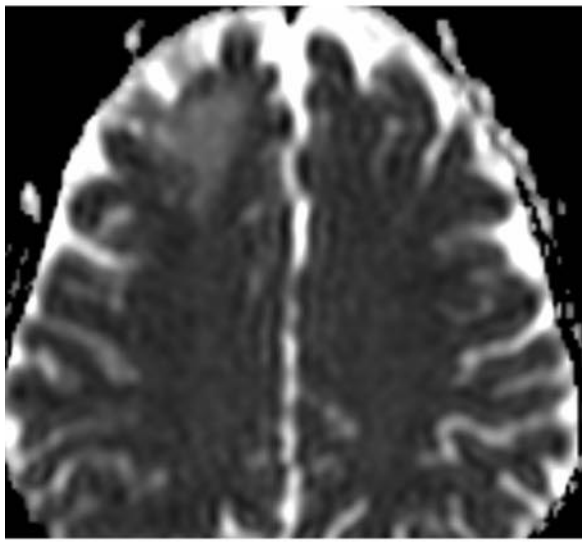

b.

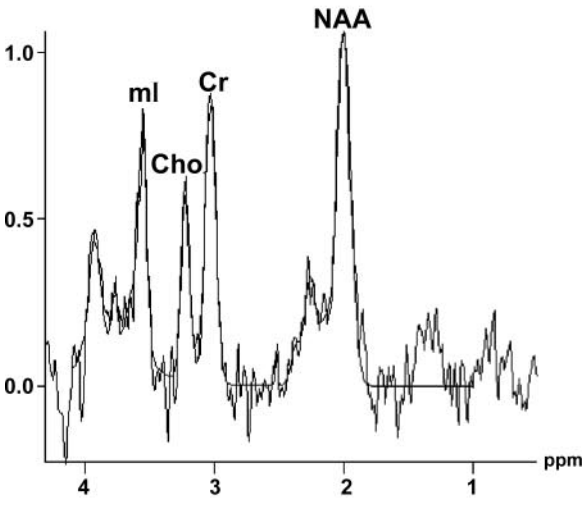

c.

Figure 4. Right frontal low-grade oligodendroglioma (WHO grade II) in a 35-year-old man. **(a)** FLAIR image shows a nonenhancing T2 hyperintense mass (similar appearance observed on postcontrast T1-weighted MR images, not shown here). **(b)** Axial ADC map shows facilitated diffusion. **(c)** Short-echo MR proton spectrum shows an elevated myoinositol *(mI)* peak (at 3.55 ppm). *Cho* = choline, *Cr* = creatine.

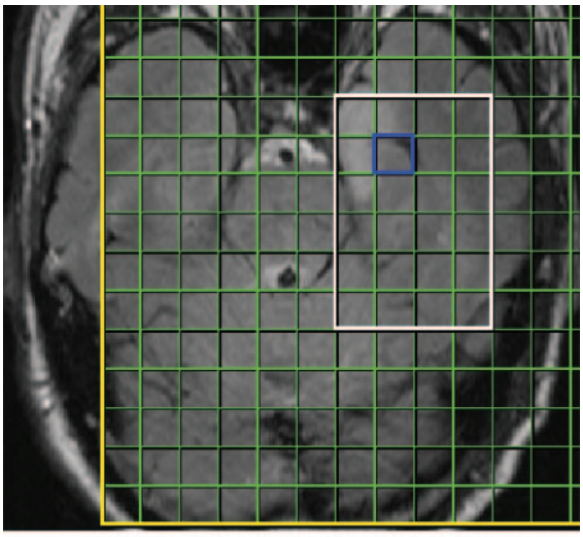

a.

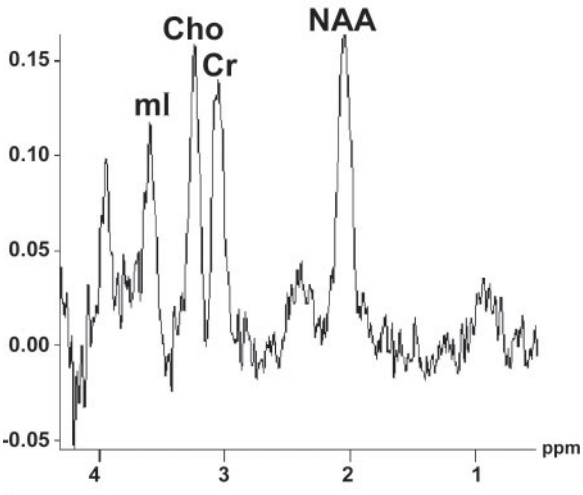

b.

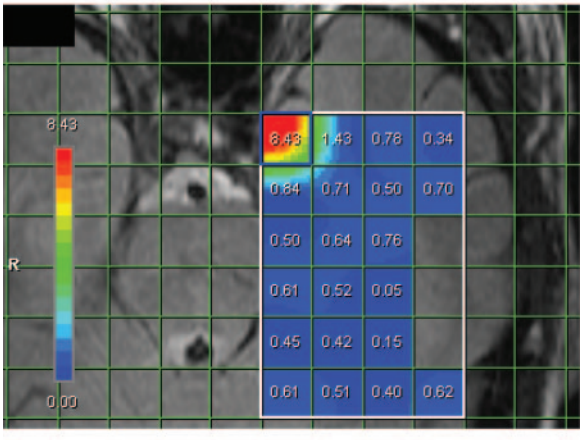

c.

Figure 5. Left temporal ganglioglioma in a 32-year-old man. **(a)** Fluid-attenuated inversion-recovery (FLAIR) MR image with overlying spectroscopic grid shows a T2 hyperintense mass. No enhancement was seen on postcontrast T1-weighted MR images (not shown). **(b)** Short-echo MR proton spectrum shows an elevated myoinositol *(mI)* peak (at 3.55 ppm). *Cho* = choline, *Cr* = creatine. **(c)** Multivoxel intermediate-echo MR proton spectroscopic color map of the choline/NAA ratio shows choline/NAA elevation.

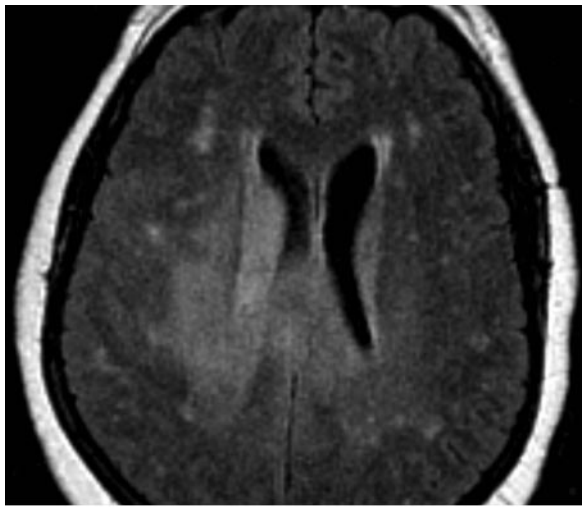

a.

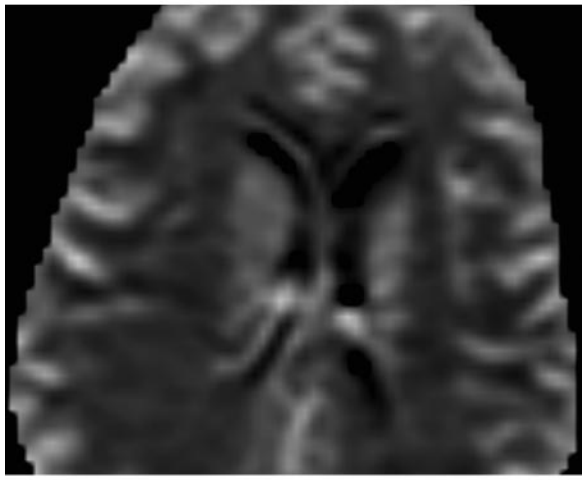

b.

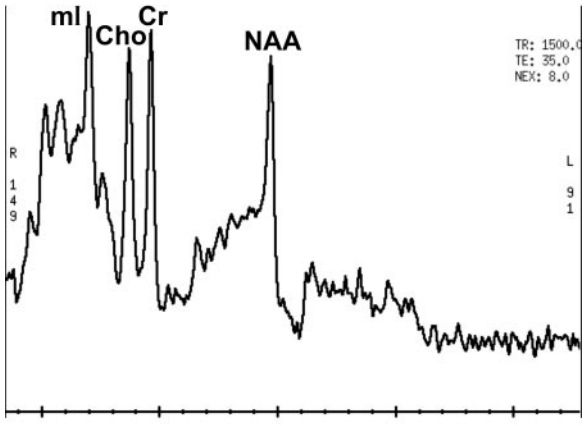

c.

Figure 6. Bihemispheric gliomatosis cerebri in a 53-year-old woman. **(a)** FLAIR image shows a T2 hyperintense nonenhancing mass involving both hemispheres (similar appearance observed on postcontrast T1-weighted MR images, not shown here). **(b)** On the axial rCBV map, the rTBV is lower than that of normal brain tissue (ratio = 0.83). **(c)** Short-echo MR proton spectrum shows elevated levels of creatine *(Cr)* (at 3.0 ppm) and myoinositol *(mI)* (at 3.55 ppm), a reduced level of NAA (at 2.02 ppm), and a mildly elevated level of choline *(Cho)* (at 3.2 ppm).

The metabolites responsible for the NAA signal are predominantly found in neurons. Thus, reduction in the NAA signal in neoplasms arises from reduced or absent production of these metabolites because normal neurons have been destroyed or displaced by the neoplastic process.

Teaching Point

The prevailing view is that an elevated choline peak is a surrogate marker of increased cell membrane turnover caused by tumor growth or normal cell destruction; however, an alternative view suggests that the choline signal may at least in part be elevated because of increased production through phospholipase upregulation.

Teaching Point

The relative anaerobic environment of many neoplasms and derangements in glucose metabolism result in incomplete glucose breakdown and likely account for the elevated lactate signal (Figs 2d, 3b) (3,4).

Teaching Point

Unfortunately, there are no unequivocal cutoff metabolite signal ratios that clearly distinguish neoplastic from nonneoplastic conditions. Published MR spectroscopic results showed a sensitivity of 79% and a specificity of 77% for a choline/NAA ratio of greater than 1 as an indicator of a neoplastic process (5). A sensitivity of 87% and a specificity of 85% were achieved by using a logistical regression model with 10 input MR spectroscopic variables (5). In our review of the literature, we were unable to find a reliable spectroscopic feature that distinguishes nonneoplastic from neoplastic conditions. However, we did find that a choline/NAA cutoff ratio of 2.2 does reliably separate high-grade neoplasms from low-grade neoplasms and nonneoplastic conditions (Figs 1c–1e, 2d, 2e, 3b, 4c).

Analysis of other metabolite peaks can also aid in grading primary neoplasms. High-grade neoplasms tend to have elevated lipid signal, which is often absent in low-grade neoplasms (Figs 2d, 3b, 4c, 5b) (6–9). On the other hand, a high myo-inositol peak is more characteristic of lower grade neoplasms and gliomatosis cerebri (the latter are WHO grade III tumors but have advanced MR imaging features that are more in line with those of low-grade neoplasms) (Fig 6c) (7).

Diffusion-weighted Imaging.—The typical diffusion-weighted imaging feature for primary neoplasms is variable apparent diffusion coefficients (ADCs) (Table). The ADC is inversely proportional to cellular density, presumably because of tortuousity of the interstitial space and the resultant limitation in water movement (10–12). Although the ADC value of high-grade gliomas has been shown to be lower than that of low-grade gliomas (13), there is substantial overlap; thus, ADC maps alone are insufficient for predicting type and grade of glial neoplasms (Figs 2b, 4b) (14). These comments may not apply to brain masses in children.

Perfusion Imaging.—The typical perfusion imaging feature for primary neoplasms is a relative tumor blood volume (rTBV) that tends to increase with neoplasm grade (Table).

Perfusion imaging allows some insight into angiogenesis, a process essential for neoplastic growth. Neoplastic induced angiogenesis results in structurally abnormal vessels that tend to be leaky, and thus neoplasms have increased permeability parameters on perfusion MR images. Several studies have shown that the grade of the neoplasm correlates with tumor blood volume (Figs 1b, 2c, 6b) (6,15–18). An rTBV of 1.75 was suggested as a cutoff threshold to distinguish a high-grade from a low-grade neoplasm (6), where rTBV is measured as a ratio of the maximal tumor blood volume to a region of interest in normal white matter. An important exception is low-grade glial neoplasms with oligodendroglial features, which may have markedly elevated rTBV (19). Markedly elevated rTBV has been observed in particular with low-grade oligodendrogliomas and oligoastrocytomas with 1p deletion.

Secondary (Metastatic) Neoplasms

MR Spectroscopy.—Typical MR spectroscopic features for secondary neoplasms include elevated signals of lipid, lactate, and choline and reduced or absent NAA signal (Table), illustrated in Figure 7.

Distinguishing metastases from high-grade primary neoplasm with spectroscopic interrogation of the enhancing portion of the tumor is unreliable, even though it has been shown by some to be possible by looking for a higher degree of lipid signal in metastatic lesions (7,8). In contrast, because primary neoplasms have the propensity to infiltrate surrounding brain tissue, interrogation of areas outside the enhancing portion of the lesion has proved to be more promising (20,21). Various metabolite signal ratios have been suggested for this purpose. In one study, a choline/NAA ratio of greater than 1 had an accuracy of 100% (20) (Fig 3).

Diffusion-weighted Imaging.—The typical diffusion-weighted imaging feature for secondary neoplasms is an elevated ADC (Table). The ADC values of metastatic lesions are variable and overlap with those of primary neoplasms (Fig 7b) (14). However, it is possible to separate metastasis from primary brain neoplasm by measuring ADC values in the peritumoral regions. Recently,

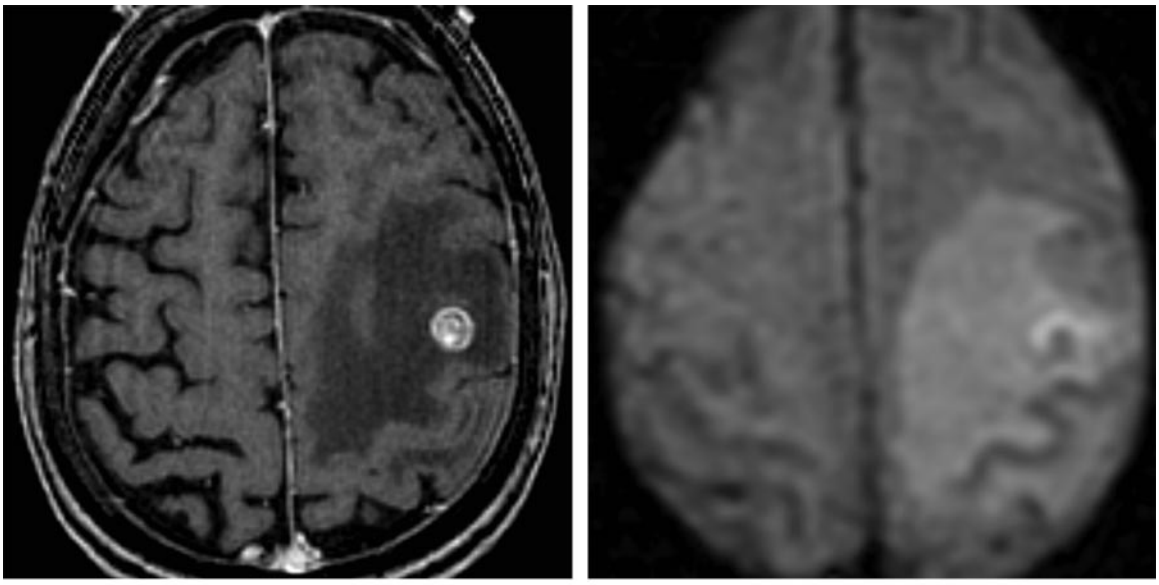

a. b.

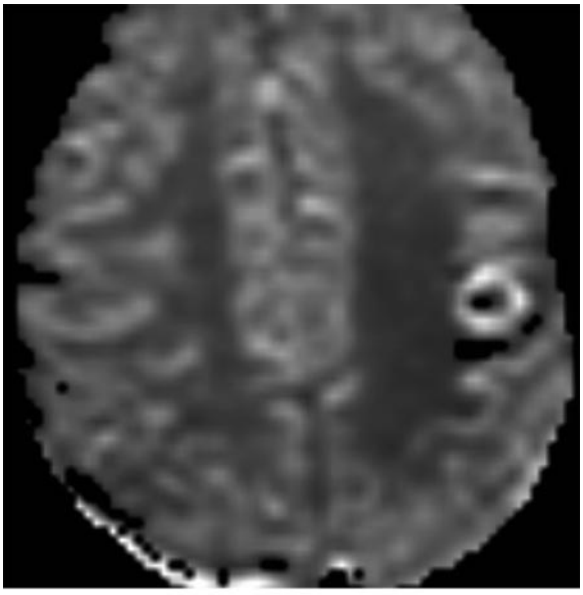

c.

Figure 7. Metastatic renal cell cancer in a 73-year-old man. **(a)** Axial postcontrast T1-weighted MR image demonstrates a heterogeneously enhancing small mass in the posterior left frontal lobe with extensive surrounding T2 hyperintensity. **(b)** Axial diffusion-weighted map shows predominantly facilitated diffusion with a small crescent-shaped area of restricted diffusion that had an ADC value of 1.04×10^{-3} mm^2/sec). **(c)** On an axial rCBV map, the rTBV is elevated (ratio = 6.27).

it has been shown that, because of neoplastic infiltration in primary neoplasms, peritumoral diffusion-tensor imaging tends to show lower ADC values in regions of peritumoral "edema" compared with those seen with metastatic disease (22).

Perfusion Imaging.—The typical perfusion imaging feature for secondary, metastatic lesions is an elevated rTBV (Table). As is the case for primary neoplasms, the ability of metastases to induce angiogenesis is crucial for metastatic lesion growth. Perfusion parameters of metastatic lesions tend to overlap with those of high-grade neoplasms, probably because of their similarity in the degree of angiogenesis. One possible feature that might allow differentiation between secondary and primary neoplasms is that metastatic lesions have lower rTBV measurements outside their enhancing portion, compared with those of the more infiltrative primary neoplasms (21,23).

Lymphoma

Primary central nervous system lymphoma accounts for 2% of extranodal lymphomas. The peak prevalence of primary central nervous system lymphoma occurs between the 5th and 6th decades of life. It is commonly associated with immunodeficiency states including acquired immunodeficiency syndrome (AIDS).

MR Spectroscopy.—Typical proton MR spectroscopic features for lymphoma include elevated signals of lipid, lactate, and choline and reduced NAA signal (Table), illustrated in Figure 8.

MR spectroscopy of lymphoma in AIDS patients revealed mild to moderately increased lactate and lipid signals, along with a prominent choline peak and decreased NAA, creatine, and myo-inositol signals (24,25). This pattern can help in differentiating lymphoma from toxoplasmosis, which typically has elevated lactate and lipid signals but absence of the other metabolites in MR spectra (26).

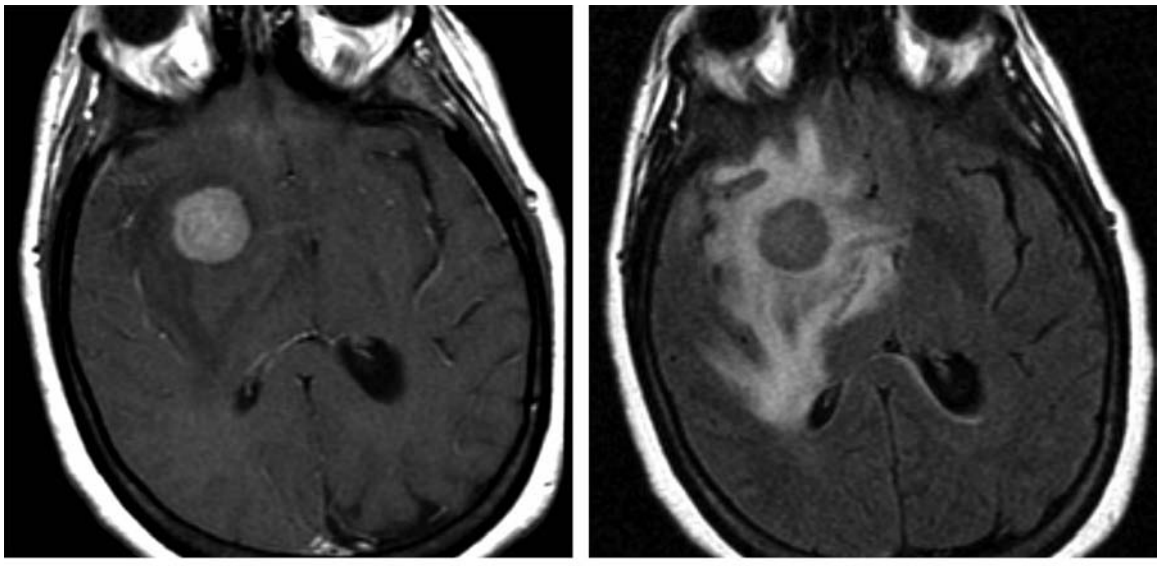

a. b.

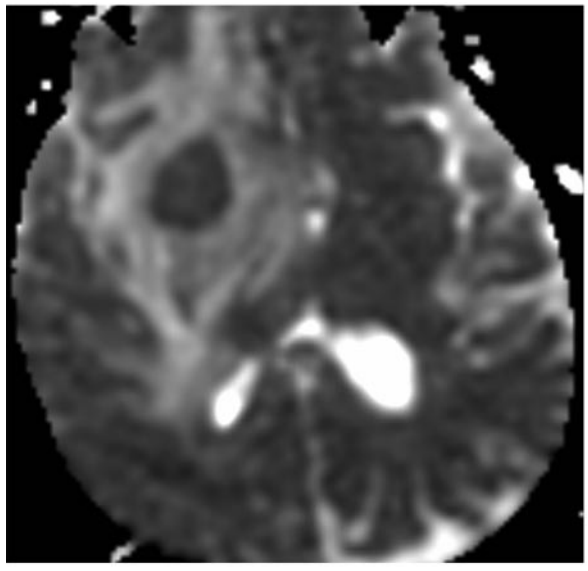

c.

Figure 8. Primary central nervous system lymphoma in a 50-year-old woman. **(a, b)** Axial postcontrast T1-weighted MR image **(a)** demonstrates a homogeneously enhancing mass in the right frontal lobe, which is isointense on the axial fluid-attenuated inversion-recovery MR image **(b),** with extensive surrounding T2 hyperintensity. **(c)** Axial ADC map shows restricted diffusion (lowest ADC value obtained was 0.82×10^{-3} mm^2/sec).

Diffusion-weighted Imaging.—The typical diffusion-weighted imaging feature for lymphoma is reduced ADC (Table). Lymphoma tends to have a low ADC due to its cellularity. This feature can help in differentiating lymphoma from toxoplasmosis, which typically has significantly greater ADC values than lymphoma lesions (Fig 8c) (27). A low ADC value would also favor lymphoma over glial tumors.

Perfusion Imaging.—The typical perfusion imaging feature for lymphoma is an rTBV that is low compared with that of primary high-grade neoplasms and high relative to toxoplasmosis (Table).

Differentiation of lymphoma and primary high-grade glial neoplasms is feasible because lymphoma tends to have a lower rTBV (23,28, 29), and the intensity time curves for lymphoma tend to be substantially below the baseline (29). However, lymphoma tends to show higher rTBV compared with toxoplasmosis (30).

Tumefactive Demyelinating Lesions

Multiple sclerosis is an autoimmune demyelinating disorder characterized by distinct episodes of neurologic deficits, separated in time and space. It affects millions of patients worldwide and approximately 250,000–350,000 in the United States alone. Symptoms usually begin during young adulthood. Acute monophasic syndromes include the Marburg variant of multiple sclerosis, Baló's concentric sclerosis, and other focal tumefactive demyelinating lesions that may simulate brain tumors. A specific diagnosis that distinguishes among these rare syndromes early in the course of disease has prognostic and treatment implications.

MR Spectroscopy.—Typical proton MR spectroscopic features for tumefactive demyelinating lesions include an elevated choline peak and reduced NAA signal (Table), as illustrated in Figure 9.

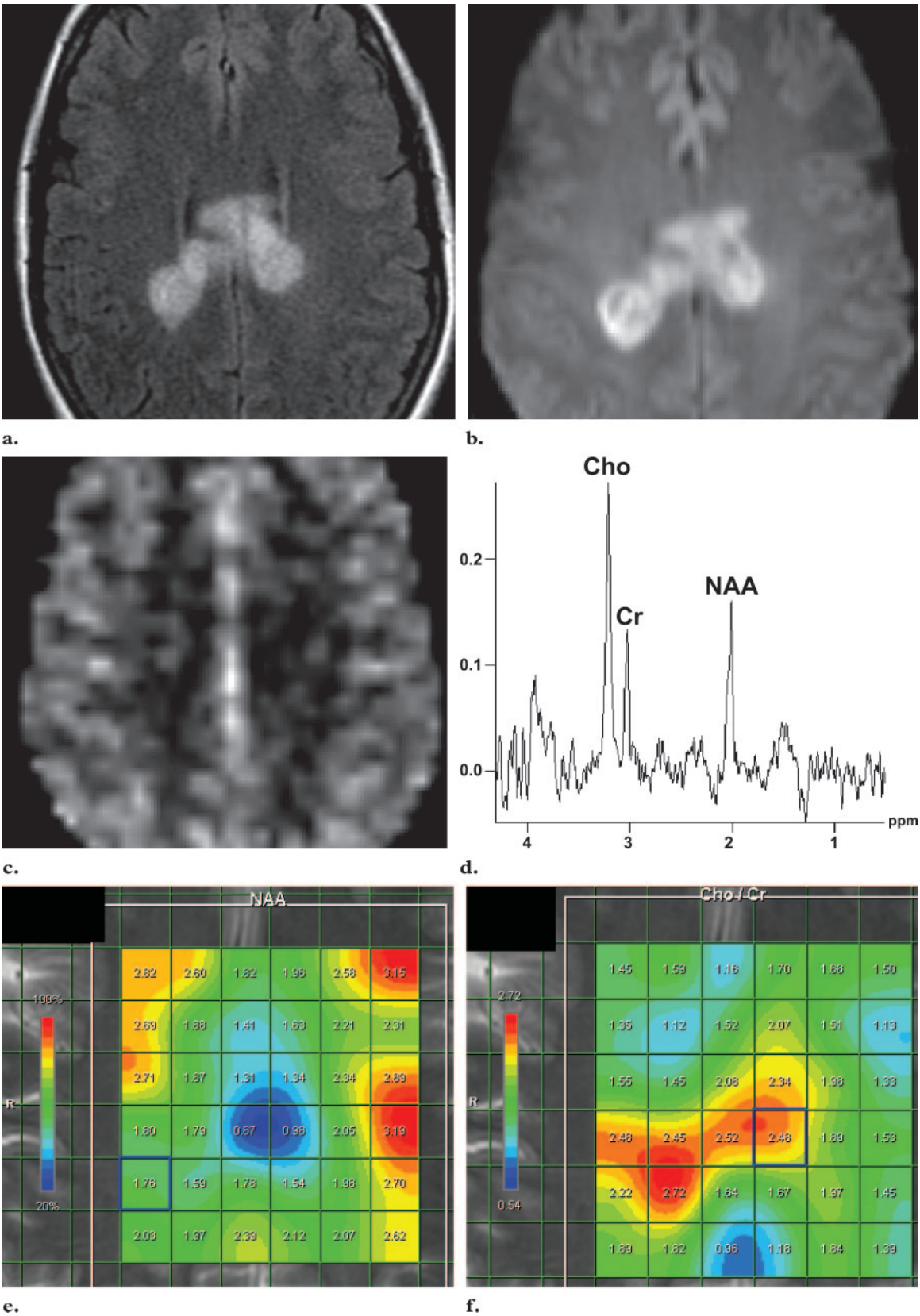

Figure 9. Periventricular tumefactive demyelinating lesion in a 38-year-old woman. **(a)** FLAIR image shows a well-defined T2 hyperintense enhancing lesion (similar appearance observed on postcontrast T1-weighted MR images, not shown here). **(b)** Axial diffusion-weighted image shows restricted diffusion. **(c)** Axial arterial spin-labeled generated cerebral blood flow map shows no elevation of flow compared with contralateral normal white matter. **(d)** Single-voxel intermediate-echo MR proton spectrum shows mild depression of the NAA peak (at 2.02 ppm), absence of the lactate peak (at 1.33 ppm), and elevation of the choline *(Cho)* peak (at 3.2 ppm). Cr = creatine. **(e, f)** These findings are further illustrated with spectroscopic color maps of NAA and the choline/creatine ratios.

A fulminant tumefactive demyelinating lesion may show high choline and low NAA signals as well as presence of lactate (31). Often, it is difficult to distinguish a tumefactive demyelinating lesion from neoplastic lesions at MR spectroscopy (Fig 9d–9f) (31,32). In multiple sclerosis, the spectroscopic abnormalities are not limited to visible lesions, since normal-appearing areas of white matter were shown to have reduced NAA signal (compared with NAA signals in healthy control subjects). In the early stages of the disease, an increased myoinositol peak may be more apparent in normal-appearing white matter than reduced NAA signal.

Diffusion-weighted Imaging.—The typical diffusion-weighted imaging feature for tumefactive demyelinating lesion is variable ADC (Table). Most tumefactive demyelinating lesions have elevated ADC values, although occasionally, acute demyelinating lesions may have areas of reduced ADC values (Fig 9b) (33).

Perfusion Imaging.—The typical perfusion imaging feature for tumefactive demyelinating lesions is a low rTBV (Table). In tumefactive demyelinating lesions, rTBV values tend to be lower than those in normal brain tissue (33). High-grade primary neoplasms and metastatic lesions have higher rTBV values than do tumefactive demyelinating lesions (Fig 9c) (23).

Brain Abscesses

Brain abscesses are rare in immunocompetent individuals. In adults, ear and sinus infections are the most common predisposing conditions for brain abscesses. On the other hand, brain abscesses may develop from hematogenous spread of infection from a distant site such as a pyogenic lung process. In addition, pulmonary arteriovenous malformation is a predisposing condition for brain abscesses.

MR Spectroscopy.—Typical MR spectroscopic features of brain abscesses include elevated peaks of amino acid, lactate, alanine, acetate, pyruvate, and succinate and absent signals of NAA, creatine, and choline (Table, Fig 10).

Abscesses have a distinct spectroscopic pattern that allows differentiation from other entities. For instance, elevation of choline (34–36) and absence of signal from a variety of amino acids, acetate, and succinate (11,36–38) are features that would favor a neoplastic process, whereas the other peaks listed above—alanine, acetate, pyruvate, and succinate—favor abscesses (Figs 1c, 2d, 10c).

MR spectroscopy may shed light on which organism is responsible for the abscess, because the presence of anaerobic bacteria tends to cause elevated acetate and succinate peaks (Fig 10c), whereas absence of acetate and succinate signals are more likely with obligate aerobes or facultative anaerobes (39,40).

Tuberculous abscesses typically have high lipid and lactate peaks. These abscesses have no peaks for amino acids (leucine, isoleucine, and valine) at 0.9 ppm, succinate at 2.41 ppm, acetate at 1.92 ppm, and alanine at 1.48 ppm, in contrast to pyogenic abscesses, which have peaks for all these metabolites.

Diffusion-weighted Imaging.—The typical diffusion-weighted imaging feature for brain abscess is markedly reduced ADC (Table). ADC maps are of great value in distinguishing neoplasms, which more often have facilitated diffusion, from abscesses, which are more likely to have restricted diffusion, in their necrotic portions (Fig 10b) (11,41,42). However, there are some reports of overlapping characteristics. Furthermore, the walls of necrotic or cystic tumors have been shown to have a lower ADC value than that of an abscess (Fig 2b, 10b) (43).

Perfusion Imaging.—The typical perfusion imaging feature for brain abscess is low rTBV (Table). High-grade primary neoplasms and metastases can be differentiated from abscesses with perfusion MR imaging, in which the wall of necrotic or cystic neoplasms tends to have higher rTBV compared with the capsule of an abscess (Figs 1b, 2c, 10d) (43).

Encephalitis

MR Spectroscopy.—Typical proton MR spectroscopic features for encephalitis include elevated peaks of lactate, choline, and myoinositol and reduced NAA signal (Table). Encephalitis tends to resemble low-grade gliomas, with reduction of the NAA signal and elevation of the choline and myoinositol peaks (44). A lactate peak is an inconsistent finding (44). After the initial acute

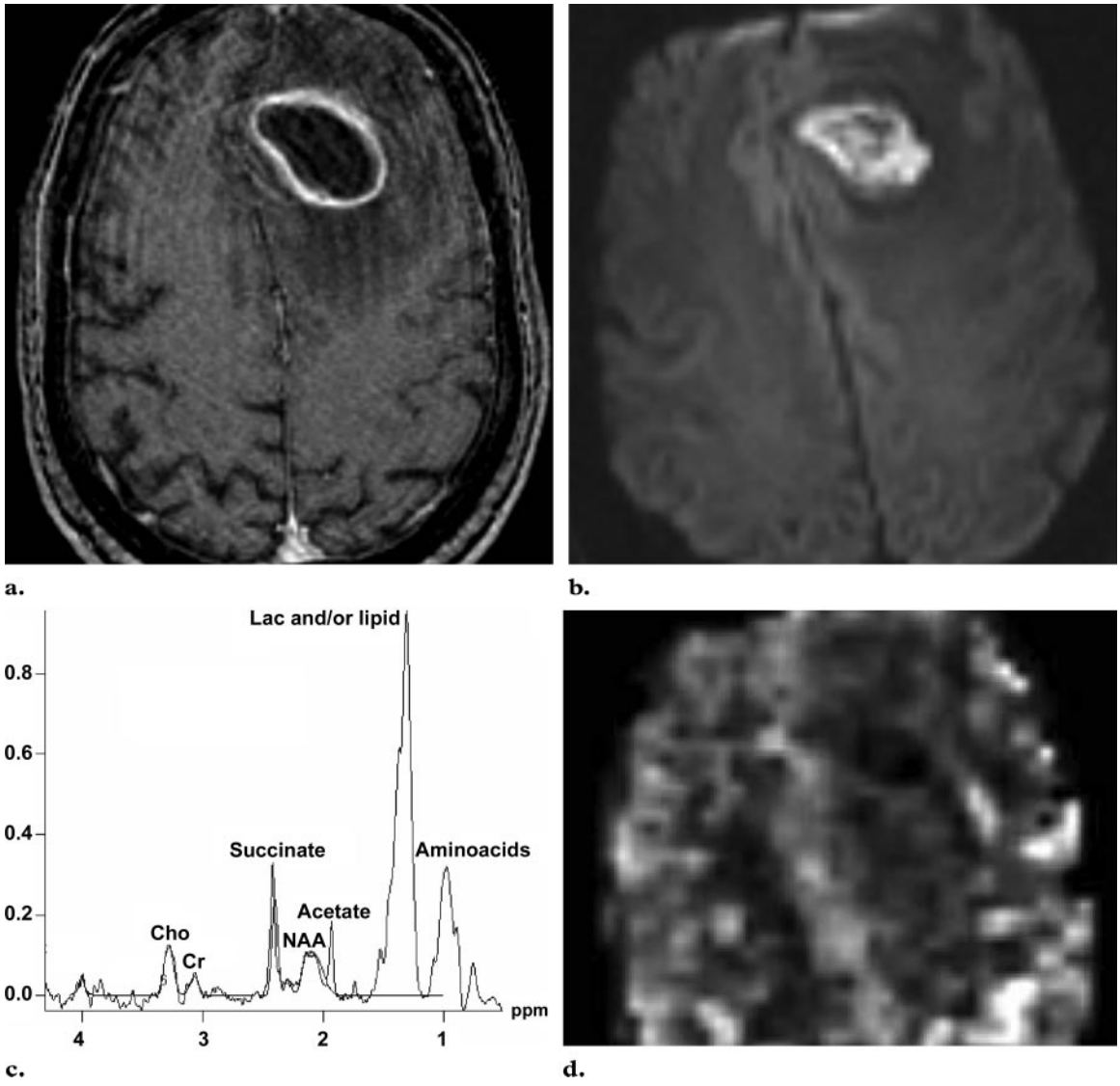

Figure 10. Left frontal abscess in a 57-year-old man. **(a)** Axial postcontrast T1-weighted MR image demonstrates a rim-enhancing mass with surrounding edema. **(b)** Axial diffusion-weighted image shows restricted diffusion with ADC measurements as low as 0.94×10^{-3} mm^2/sec, corresponding to the nonenhancing portion of the abscess. **(c)** Short-echo MR spectrum shows depression of the NAA (at 2.02 ppm), choline *(Cho)* (at 3.2 ppm), and creatine *(Cr)* (at 3.0 ppm) peaks, as well as elevation of the amino acid (at 0.9 ppm), lactate *(Lac)* (at 1.33 ppm), acetate (at 1.9 ppm), and succinate (at 2.4 ppm) peaks. **(d)** Axial arterial spin-labeled generated cerebral blood flow map shows no elevation of flow compared with contralateral normal white matter.

phase of encephalitis, there is gradual normalization of the MR spectrum in about 1 year (45).

Diffusion-weighted Imaging.—The typical diffusion-weighted imaging feature for encephalitis is variable ADC (Table). Encephalitis typically has low ADC values. However, this finding is not as consistent as that seen with infarcted tissue (46). Diffusion-weighted imaging may also shed light on the severity of the process, because fulminant cases are more likely to cause restricted diffusion (44).

Perfusion Imaging.—The typical perfusion imaging feature for encephalitis is unknown. To our knowledge, there has been no report in the literature on perfusion MR imaging of encephalitis. A case report of perfusion computed tomography suggests elevated perfusion in the acute phase (47). The nuclear medicine literature describes normal to elevated perfusion initially, followed by abnormal reduction in the chronic phase (48).

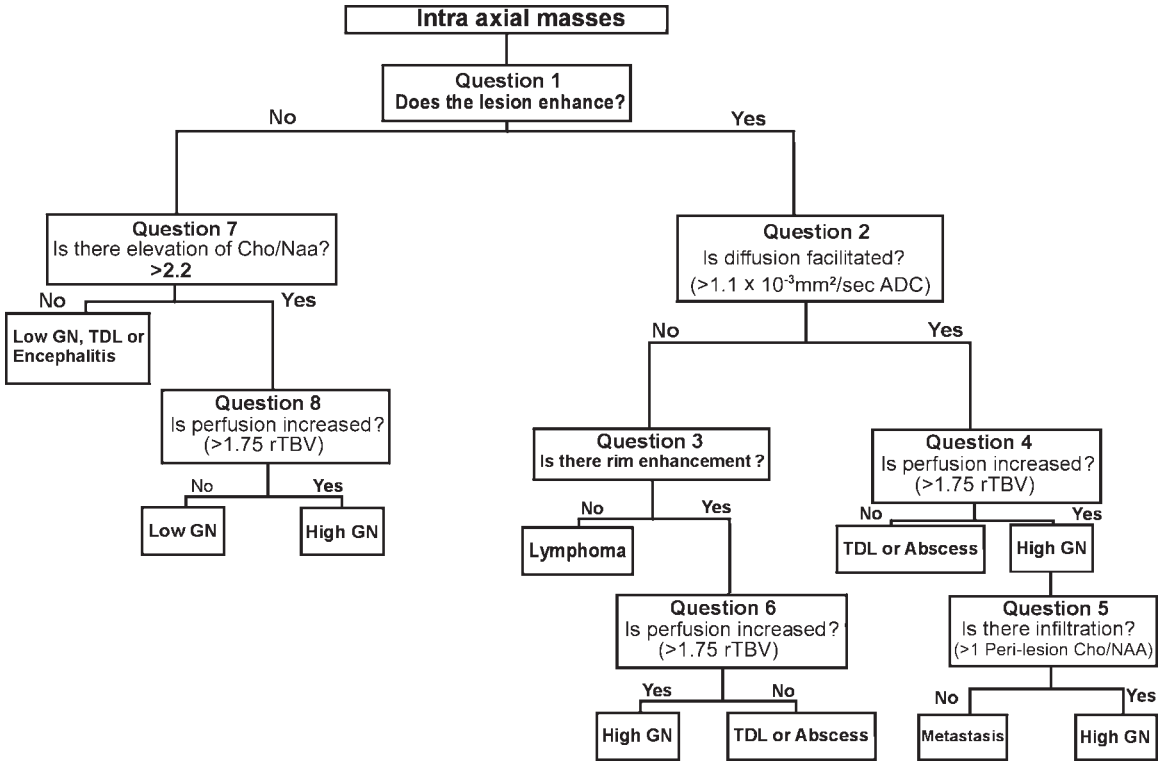

Figure 11. Algorithm for unknown intracranial mass classification. This practical MR imaging algorithm is composed of a series of nodes or questions that would suggest a diagnosis if the paths are followed to the bottom. *Cho* = choline, *High GN* = high-grade neoplasm, *Low GN* = low-grade neoplasm, *TDL* = tumefactive demyelinating lesion.

Integrated Conventional and Advanced MR Imaging Diagnostic Approach to Intraaxial Masses

Figure 11 shows an algorithm designed to help classify unknown intraaxial lesions in immunocompetent adults. Low-grade primary neoplasm, high-grade primary neoplasm, metastatic neoplasm, lymphoma, tumefactive demyelinating lesion, abscess, and encephalitis are common intraaxial masses that represent the diagnostic endpoints of this algorithm.

The algorithm contains several questions whose answers require information derived from MR imaging studies.

Question 1: Does the Lesion Enhance at Conventional MR Imaging?—An assessment of whether the lesion is intraaxial or extraaxial is crucial as an initial step. Simple visual inspection is performed to assess for any perceived enhancement.

The general purpose at this point is to discriminate typically nonenhancing lesions such as low-grade neoplasms and encephalitis from typically enhancing lesions such as abscesses, lymphomas, tumefactive demyelinating lesions, high-grade primary neoplasms, and metastatic lesions (49). Admittedly, contrast enhancement is not specific, as it represents disruption of the blood-brain barrier; however, it is commonly used in clinical practice as an initial discriminator to improve lesion detection and differentiation (49).

Question 2: Is Diffusion Facilitated, as Determined with Diffusion-weighted Imaging?—At this point, the lowest ADC value (expressed $\times 10^{-3}$ mm^2/sec) should be recorded from several regions of interest within the lesion, including both enhancing and nonenhancing parts, regardless of whether that part was solid or cystic.

The primary purpose is to separate lesions that typically have reduced diffusion such as lymphomas and abscesses from lesions that typically have

facilitated diffusion such as neoplasms and tumefactive demyelinating lesions (42). There is no universally accepted threshold for ADC to determine whether diffusion is facilitated or not; however, after a meta-analysis of publications from different centers, we adopted a value of 1.1×10^{-3} mm^2/sec (11,27,41,42).

Question 3: Is There Rim Enhancement or Necrosis at Conventional Postcontrast MR Imaging?—Presence of necrosis is indicated by a nonenhancing area, which is dark on T1-weighted images, bright on T2-weighted images, and surrounded by enhancing tissue.

This question helps differentiate lymphomas, which typically lack rim enhancement in immunocompetent patients before therapy, from tumefactive demyelinating lesions, abscesses, and high-grade neoplasms, in which central necrosis and peripheral enhancement are common.

Question 4: In Lesions with Facilitated Diffusion, Is Perfusion Increased?—Perfusion measurements are made from several regions of interest within the lesion and compared with values obtained in normal white matter. The highest rTBV is recorded from several regions of interest, including both enhancing and nonenhancing portions of the mass, regardless of whether the portion is solid or cystic.

There is no universally accepted single threshold for rTBV that can help discriminate among the various intraaxial lesions. In a cohort of tumefactive demyelinating lesion cases, the highest rTBV was 1.79 (50). As previously indicated, neoplastic lesions tend to have higher rTBV (2.90 ± 0.62) compared with abscesses (0.45 ± 0.11) (43). In a separate study, the use of an rTBV threshold of 1.75 to distinguish high-grade neoplasm from low-grade glial neoplasms resulted in the lowest C2 type error and a sensitivity of 95.0% and a specificity of 57.5% (6). Therefore, this threshold is used at this point in the algorithm.

The purpose here is to differentiate tumefactive demyelinating lesions and abscesses from high-grade neoplasms and metastases. Primary high-grade neoplasms and metastases are expected to have an elevated rTBV (in contrast to tumefactive demyelinating lesions, abscesses, and low-grade neoplasms) because of differences in angiogenesis induction (6,18,43,50).

Question 5: Is There Infiltration of Surrounding Tissue?—As previously indicated, metastases tend not to infiltrate surrounding tissue (5,43,44); thus, spectroscopic interrogation of peritumoral tissue can be more effective for differential diagnosis than measurements from enhancing tissue (20). There is no universal discriminating threshold for the choline/NAA ratio; however, a ratio of 1.0 was shown to have 100% accuracy for differentiating between primary and secondary neoplasms when correlated with results of stereotactic biopsies in one study (20).

Question 6: In Lesions with Reduced Diffusion and Rim Enhancement, Is Perfusion Increased?—As previously indicated, neoplastic lesions tend to have higher rTBV compared with that of abscesses (43). The threshold of 1.75 used in Question 4 is used at this point for the sake of simplicity.

Question 7: Is There Elevation of Choline/NAA Ratio?—Despite overlap of MR spectroscopic ratios for encephalitis, tumefactive demyelinating lesions, and gliomas (6,8,20,24,32), we used a choline/NAA ratio of 2.2 to separate primary high-grade neoplasms from mimicking lesions such as encephalitis and tumefactive demyelinating lesions. This value was calculated through a meta-analysis of published choline/NAA ratios for high-grade gliomas, tumefactive demyelinating lesions, and encephalitis (6,8,20,24,32). Those cases in which the response to this question is "no" are an imaging challenge, and clinical and imaging follow-up or a biopsy certainly has a role for further discrimination.

Question 8: In Nonenhancing Lesions, Is Perfusion Increased?—The threshold of 1.75 used in Questions 4 and 6 is used at this point in the algorithm. Perfusion imaging has better accuracy than MR spectroscopy and ADC for grading primary brain neoplasms (6).

Conclusions

Intraaxial brain masses are a significant health problem and are often a diagnostic imaging challenge. Knowledge of the most common intraaxial masses and familiarity with their advanced MR

imaging characteristics can substantially and noninvasively improve the accuracy in diagnosis and classification of these masses.

References

1. Tilgner J, Herr M, Ostertag C, Volk B. Validation of intraoperative diagnoses using smear preparations from stereotactic brain biopsies: intraoperative versus final diagnosis—influence of clinical factors. Neurosurgery 2005;56(2):257–263.
2. Perez-Cruet MJ, Adelman L, Anderson M, Roth PA, Ritter AM, Saris SC. CT-guided stereotactic biopsy of nonenhancing brain lesions. Stereotact Funct Neurosurg 1993;61(3):105–117.
3. Negendank WG, Sauter R, Brown TR, et al. Proton magnetic resonance spectroscopy in patients with glial tumors: a multicenter study. J Neurosurg 1996;84(3):449–458.
4. Tien RD, Lai PH, Smith JS, Lazeyras F. Single-voxel proton brain spectroscopy exam (PROBE/SV) in patients with primary brain tumors. AJR Am J Roentgenol 1996;167(1):201–209.
5. Butzen J, Prost R, Chetty V, et al. Discrimination between neoplastic and nonneoplastic brain lesions by use of proton MR spectroscopy: the limits of accuracy with a logistic regression model. AJNR Am J Neuroradiol 2000;21(7):1213–1219.
6. Law M, Yang S, Wang H, et al. Glioma grading: sensitivity, specificity, and predictive values of perfusion MR imaging and proton MR spectroscopic imaging compared with conventional MR imaging. AJNR Am J Neuroradiol 2003;24(10):1989–1998.
7. Howe FA, Barton SJ, Cudlip SA, et al. Metabolic profiles of human brain tumors using quantitative in vivo H-1 magnetic resonance spectroscopy. Magn Reson Med 2003;49(2):223–232.
8. Moller-Hartmann W, Herminghaus S, Krings T, et al. Clinical application of proton magnetic resonance spectroscopy in the diagnosis of intracranial mass lesions. Neuroradiology 2002;44(5):371–381.
9. Galanaud D, Chinot O, Nicoli F, et al. Use of proton magnetic resonance spectroscopy of the brain to differentiate gliomatosis cerebri from low-grade glioma. J Neurosurg 2003;98(2):269–276.
10. Gupta RK, Sinha U, Cloughesy TF, Alger JR. Inverse correlation between choline magnetic resonance spectroscopy signal intensity and the apparent diffusion coefficient in human glioma. Magn Reson Med 1999;41(1):2–7.
11. Lai PH, Ho JT, Chen WL, et al. Brain abscess and necrotic brain tumor: discrimination with proton MR spectroscopy and diffusion-weighted imaging. AJNR Am J Neuroradiol 2002;23(8):1369–1377.
12. Chenevert TL, Stegman LD, Taylor JM, et al. Diffusion magnetic resonance imaging: an early surrogate marker of therapeutic efficacy in brain tumors. J Natl Cancer Inst 2000;92(24):2029–2036.
13. Yang D, Korogi Y, Sugahara T, et al. Cerebral gliomas: prospective comparison of multivoxel 2D chemical-shift imaging proton MR spectroscopy, echoplanar perfusion and diffusion-weighted MRI. Neuroradiology 2002;44(8):656–666.
14. Lam WW, Poon WS, Metreweli C. Diffusion MR imaging in glioma: does it have any role in the preoperation determination of grading of glioma? Clin Radiol 2002;57(3):219–225.
15. Aronen HJ, Pardo FS, Kennedy DN, et al. High microvascular blood volume is associated with high glucose uptake and tumor angiogenesis in human gliomas. Clin Cancer Res 2000;6(6):2189–2200.
16. Aronen HJ, Glass J, Pardo FS, et al. Echo-planar MR cerebral blood-volume mapping of gliomas: clinical utility. Acta Radiol 1995;36(5):520–528.
17. Aronen HJ, Gazit IE, Louis DN, et al. Cerebral blood-volume maps of gliomas: comparison with tumor grade and histologic findings. Radiology 1994;191(1):41–51.
18. Knopp EA, Cha S, Johnson G, et al. Glial neoplasms: dynamic contrast-enhanced T2*-weighted MR imaging. Radiology 1999;211(3):791–798.
19. Lev MH, Ozsunar Y, Henson JW, et al. Glial tumor grading and outcome prediction using dynamic spin-echo MR susceptibility mapping compared with conventional contrast-enhanced MR: confounding effect of elevated rCBV of oligodendrogliomas. AJNR Am J Neuroradiol 2004;25:214–221.
20. Burtscher IM, Skagerberg G, Geijer B, Englund E, Stahlberg F, Holtas S. Proton MR spectroscopy and preoperative diagnostic accuracy: an evaluation of intracranial mass lesions characterized by stereotactic biopsy findings. AJNR Am J Neuroradiol 2000;21(1):84–93.
21. Law M, Cha S, Knopp EA, Johnson G, Arnett J, Litt AW. High-grade gliomas and solitary metastases: differentiation by using perfusion and proton spectroscopic MR imaging. Radiology 2002;222(3):715–721.
22. Lu S, Ahn D, Johnson G, Cha S. Peritumoral diffusion tensor imaging of high-grade gliomas and metastatic brain tumors. AJNR Am J Neuroradiol 2003;24(5):937–941.
23. Cha S, Knopp EA, Johnson G, Wetzel SG, Litt AW, Zagzag D. Intracranial mass lesions: dynamic contrast-enhanced susceptibility-weighted echo-planar perfusion MR imaging. Radiology 2002;223(1):11–29.

24. Chang L, Miller BL, McBride D, et al. Brain lesions in patients with AIDS: H-1 MR spectroscopy. Radiology 1995;197(2):525–531. [Published correction appears in Radiology 1996;198(2):586.]
25. Simone IL, Federico F, Tortorella C, et al. Localised H-1-MR spectroscopy for metabolic characterisation of diffuse and focal brain lesions in patients infected with HIV. J Neurol Neurosurg Psychiatry 1998;64(4):516–523.
26. Chinn RJ, Wilkinson ID, Hall Craggs MA, et al. Toxoplasmosis and primary central nervous system lymphoma in HIV infection: diagnosis with MR spectroscopy. Radiology 1995;197(3):649–654.
27. Camacho DL, Smith JK, Castillo M. Differentiation of toxoplasmosis and lymphoma in AIDS patients by using apparent diffusion coefficients. AJNR Am J Neuroradiol 2003;24(4):633–637.
28. Sugahara T, Korogi Y, Shigematsu Y, et al. Value of dynamic susceptibility contrast magnetic resonance imaging in the evaluation of intracranial tumors. Top Magn Reson Imaging 1999;10(2):114–124.
29. Hartmann M, Heiland S, Harting I, et al. Distinguishing of primary cerebral lymphoma from high-grade glioma with perfusion-weighted magnetic resonance imaging. Neurosci Lett 2003;338(2):119–122.
30. Ernst TM, Chang L, Witt MD, et al. Cerebral toxoplasmosis and lymphoma in AIDS: perfusion MR imaging experience in 13 patients. Radiology 1998;208(3):663–669.
31. Bitsch A, Bruhn H, Vougioukas V, et al. Inflammatory CNS demyelination: histopathologic correlation with in vivo quantitative proton MR spectroscopy. AJNR Am J Neuroradiol 1999;20(9):1619–1627.
32. Saindane AM, Cha S, Law M, Xue X, Knopp EA, Zagzag D. Proton MR spectroscopy of tumefactive demyelinating lesions. AJNR Am J Neuroradiol 2002;23(8):1378–1386.
33. Bernarding J, Braun J, Koennecke HC. Diffusion- and perfusion-weighted MR imaging in a patient with acute demyelinating encephalomyelitis (ADEM). J Magn Reson Imaging 2002;15(1):96–100.
34. Gupta RK, Pandey R, Khan EM, Mittal P, Gujral RB, Chhabra DK. Intracranial tuberculomas: MRI signal intensity correlation with histopathology and localised proton spectroscopy. Magn Reson Imaging 1993;11(3):443–449.
35. Yamagata NT, Miller BL, McBride D, et al. In vivo proton spectroscopy of intracranial infections and neoplasms. J Neuroimaging 1994;4(1):23–28.
36. Remy C, Lebars E, Ibarrola D, Lai ES, Grand S, Decorps M. In-vivo imaging of metabolites using nuclear-magnetic-resonance spectroscopy. J Trace Microprobe Tech 1995;13(3):293–301.
37. Grand S, Passaro G, Ziegler A, et al. Necrotic tumor versus brain abscess: importance of amino acids detected at 1H MR spectroscopy—initial results. Radiology 1999;213(3):785–793.
38. Burtscher IM, Holtas S. In vivo proton MR spectroscopy of untreated and treated brain abscesses. AJNR Am J Neuroradiol 1999;20(6):1049–1053.
39. Garg M, Gupta RK, Husain M, et al. Brain abscesses: etiologic categorization with in vivo proton MR spectroscopy. Radiology 2004;230(2):519–527.
40. Lai PH, Li KT, Hsu SS, et al. Pyogenic brain abscess: findings from in vivo 1.5-T and 11.7-T in vitro proton MR spectroscopy. AJNR Am J Neuroradiol 2005;26(2):279–288.
41. Chang SC, Lai PH, Chen WL, et al. Diffusion-weighted MRI features of brain abscess and cystic or necrotic brain tumors: comparison with conventional MRI. Clin Imaging 2002;26(4):227–236.
42. Ebisu T, Tanaka C, Umeda M, et al. Discrimination of brain abscess from necrotic or cystic tumors by diffusion-weighted echo planar imaging. Magn Reson Imaging 1996;14(9):1113–1116.
43. Chan JH, Tsui EY, Chau LF, et al. Discrimination of an infected brain tumor from a cerebral abscess by combined MR perfusion and diffusion imaging. Comput Med Imaging Graph 2002;26(1):19–23.
44. Sener RN. Rasmussen's encephalitis: proton MR spectroscopy and diffusion MR findings. J Neuroradiol 2000;27(3):179–184.
45. Takanashi J, Sugita K, Ishii M, Aoyagi M, Niimi H. Longitudinal MR imaging and proton MR spectroscopy in herpes simplex encephalitis. J Neurol Sci 1997;149(1):99–102.
46. Tsuchiya K, Katase S, Yoshino A, Hachiya J. Diffusion-weighted MR imaging of encephalitis. AJR Am J Roentgenol 1999;173(4):1097–1099.
47. Nonaka M, Ariyoshi N, Shonai T, et al. CT perfusion abnormalities in a case of non-herpetic acute limbic encephalitis [in Japanese]. Rinsho Shinkeigaku 2004;44(8):537–540.
48. Launes J, Lindroth L, Liewendahl K, Nikkinen P, Brownell AL, Iivanainen M. Diagnosis of acute herpes simplex encephalitis by brain perfusion single photon emission computed tomography. Lancet 1988;1(8596):1188–1191.
49. Runge VM, Muroff LR, Jinkins JR. Central nervous system: review of clinical use of contrast media. Top Magn Reson Imaging 2001;12(4):231–263.
50. Cha S, Pierce S, Knopp EA, et al. Dynamic contrast-enhanced T2*-weighted MR imaging of tumefactive demyelinating lesions. AJNR Am J Neuroradiol 2001;22(6):1109–1116.

Advanced MR Imaging Techniques in the Diagnosis of Intraaxial Brain Tumors in Adults

Riyadh N. Al-Okaili, MD, et al

RadioGraphics 2006; 26:S173–S189 • **Published online** 10.1148/rg.26si065513 • **Content Codes:** MR NR OI

Page S180
Reduction in the NAA signal in neoplasms arises from reduced or absent production of these matabolites because normal neurons have been destroyed or displaced by the neoplastic process.

Page S180
The prevailing view is that an elevated choline peak is a surrogate marker of increased cell membrane turnover caused by tumor growth or normal cell destruction; however, an alternative view suggests that the choline signal may at least in part be elevated because of increased production through phospholipase upregulation.

Page S180
The relative anaerobic environment of many neoplasms and derangements in glucose metabolism result in incomplete glucose breakdown and likely account for the elevated lactate signal.